Electrophilic aromatic substitution reactions of compounds with Craig-Möbius aromaticity

Yuanting Cai[a,1], Yuhui Hua[a,b,1], Zhengyu Lu[a,b], Qing Lan[a], Zuzhang Lin[a], Jiawei Fei[a], Zhixin Chen[a], Hong Zhang[a,2], and Haiping Xia[a,b,2]

[a]State Key Laboratory of Physical Chemistry of Solid Surfaces, Collaborative Innovation Center of Chemistry for Energy Materials, College of Chemistry and Chemical Engineering, Xiamen University, Xiamen, China 361005; and [b]Shenzhen Grubbs Institute and Department of Chemistry, Southern University of Science and Technology, Shenzhen, China 518005

Edited by Dean J. Tantillo, University of California Davis, Davis, CA, and accepted by Editorial Board Member Tobin J. Marks August 3, 2021 (received for review February 4, 2021)

Electrophilic aromatic substitution (EAS) reactions are widely regarded as characteristic reactions of aromatic species, but no comparable reaction has been reported for molecules with Craig-Möbius aromaticity. Here, we demonstrate successful EAS reactions of Craig-Möbius aromatics, osmapentalenes, and fused osmapentalenes. The highly reactive nature of osmapentalene makes it susceptible to electrophilic attack by halogens, thus osmapentalene, osmafuran-fused osmapentalene, and osmabenzene-fused osmapentalene can undergo typical EAS reactions. In addition, the selective formation of a series of halogen substituted metalla-aromatics via EAS reactions has revealed an unprecedented approach to otherwise elusive compounds such as the unsaturated cyclic chlorirenium ions. Density functional theory calculations were conducted to study the electronic effect on the regioselectivity of the EAS reactions.

electrophilic aromatic substitution | Craig-Möbius aromaticity | hypervalent iodine reagents | unsaturated chlorirenium ion

Aromaticity, a core concept in chemistry, was initially introduced to account for the bonding, stability, reactivity, and other properties of many unsaturated organic compounds. There have been many elaborations and extensions of the concept of aromaticity (1, 2). The concepts of Hückel aromaticity and Möbius aromaticity are widely accepted (Fig. 1*A*). A π-aromatic molecule of the Hückel type is planar and has $4n + 2$ conjugated π-electrons ($n = 0$ or an integer), whereas a Möbius aromatic molecule has one twist of the π-system, similar to that in a Möbius strip, and $4n$ π-electrons (3, 4). Since the discovery of naphthalene in 1821, aromatic chemistry has developed into a rich field and with a variety of subdisciplines over the course of its 200-y history, and the concept of aromaticity has been extended to other nontraditional structures with "cyclic delocalization of mobile electrons" (5). For example, benzene-like metallacycles—predicted by Hoffmann et al. as metallabenzenes—in which a metal replaces a C–H group in the benzene ring (6), have garnered extensive research interest from both experimentalists and theoreticians (7–12). As paradigms of the metalla-aromatic family, most complexes involving metallabenzene exhibit thermodynamic stability, kinetic persistence, and chemical reactivity associated with the classical aromaticity concept (13–15). Typically, like benzene, metallabenzene can undergo characteristic reactions of aromatics such as electrophilic aromatic substitution (EAS) reactions (16–18) (Fig. 1*B*, I) and nucleophilic aromatic substitution reactions (19–21).

The incorporation of transition metals has also led to an increase in the variety of the aromatic families (22–25). We have reported that stable and highly unusual bicyclic systems, metallapentalenes (osmapentalenes), benefit from Craig-Möbius aromaticity (26–30). In contrast to other reported Möbius aromatic compounds with twisted topologies, which are known as Heilbronner-Möbius aromatics (31–34), the involvement of transition metal d orbitals in π-conjugation switches the Hückel anti-aromaticity of pentalene into the planar Craig-Möbius aromaticity of metallapentalene (35–38) (Fig. 1*A*, III). Both the twisted topology and the planar Craig-Möbius aromaticity are well established and have been accepted as reasonable extensions of aromaticity (39–43). There has been no experimental evidence, however, as to whether these Möbius aromatic molecules can undergo classical aromatic substitution reactions, such as EAS reactions, instead of addition reactions. Given the key role of EAS in aromatic chemistry to obtain various derivatives, we sought to extend the understanding of the reactivity paradigm in the metalla-aromatic family.

Our recent synthetic efforts associated with the metallapentalene system prompted us to investigate whether typical EAS reactions could proceed in these Craig-Möbius aromatics. If so, how could substitution be achieved in the same way that it is with traditional Hückel aromatics such as benzenes? In this paper, we present EAS reactions, mainly the halogenation of osmapentalene, osmafuran-fused osmapentalene, and osmabenzene-fused osmapentalene, which follow the classic EAS mechanistic scheme (Fig. 1*B*). With the aid of density functional theory (DFT) calculations, we characterized the effects on EAS reactivity and regioselectivity.

Significance

Electrophilic aromatic substitution (EAS) reactions are hallmarks of aromaticity. However, the potential of compounds with Möbius aromaticity to undergo EAS has been ignored for a long time. A number of molecules with d orbitals involved in conjugation of π-aromatic ring in the out-of-phase way have been described as Craig-Möbius aromaticity because they have the same phase inversion properties as Möbius type and fit [4n] rule. Embedding metals within a π-conjugated hydrocarbon skeleton is considered an efficient method for discovering Craig-Möbius aromatic scaffolds. We directly employed metalla-aromatics to develop EAS reactions of Craig-Möbius aromatics with excellent efficiency and remarkable regioselectivity, and the reactions were quantified in computational studies to further rationalize the preferred sites of attack on the different aromatic rings.

Author contributions: Y.C., Y.H., Z. Lu, Q.L., Z. Lin, and J.F. performed research; H.Z. and H.X. designed research; Z.C. contributed new reagents/analytic tools; Y.C., Y.H., H.Z., and H.X. analyzed data; and Y.C., H.Z., and H.X. wrote the paper.

The authors declare no competing interest.

This article is a PNAS Direct Submission. D.J.T. is a guest editor invited by the Editorial Board.

[1]Y.C. and Y.H. contributed equally to this work.

[2]To whom correspondence may be addressed. Email: xiahp@sustech.edu.cn or zh@xmu.edu.cn.

This article contains supporting information online at https://www.pnas.org/lookup/suppl/doi:10.1073/pnas.2102310118/-/DCSupplemental.

Published September 20, 2021.

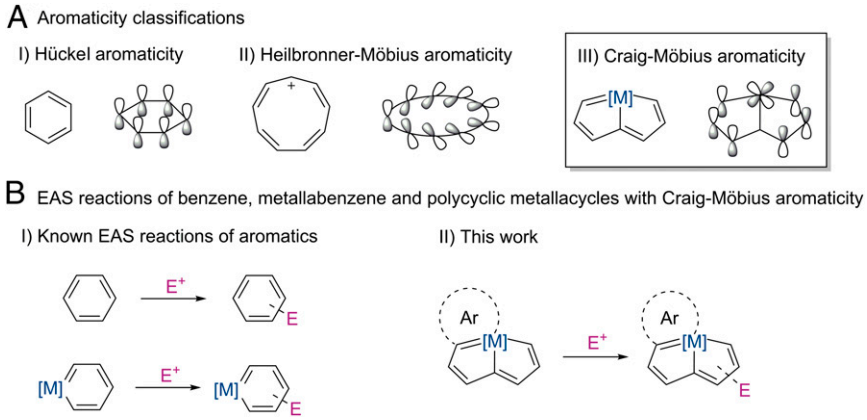

Fig. 1. Schematic representations of aromaticity classification (*A*) and EAS reactions (*B*) of benzene, metallabenzene, and polycyclic metallacycles with Craig-Möbius aromaticity.

Results and Discussion

EAS Reactions of Osmapentalene. With the goal of carrying out EAS reactions with metallapentalene, we first examined halogenation, a prototypical EAS reaction. Taking a cue from the importance of hypervalent iodine reagents in halogenation reactions (44–46), air- and moisture-stable halobenzo-iodaoxoles were employed as electrophilic halogen reagents for osmapentalene (**1**). As shown in Fig. 2, treatment of osmapentalene (**1**) with 1-chloro-3,3-dimethyl-1,3-dihydro-1λ^3-benzo[*d*][1,2]iodaoxole at room temperature (RT) under nitrogen cleanly afforded complex **2** in 15 min. In situ NMR studies of **2** produced diagnostic ^{1}H NMR resonances at 13.58 (H1), 9.54 (H3), and 8.94 ppm (H5), and ^{13}C{^{1}H} NMR resonances at 226.4 (C1), 224.6 (C7), 188.7 (C4), 165.2 (C5), 162.8 (C3), 150.1 (C6), and 138.7 ppm (C2), which are similar to those seen for other osmapentalene compounds (47). Golden yellow crystals of **2** suitable for X-ray diffraction analysis were grown by diffusion of hexane into a dichloromethane solution, and the chloro-osmapentalene product was confirmed to be monosubstituted (Fig. 2*A*). The structural analyses clearly revealed that the metal center in **2** has a pentagonal bipyramidal geometry, and the equatorial polycyclic ring system (rings a, b, and c) is nearly coplanar, as reflected by the small mean deviation from the least-squares plane (0.010 Å). The bond lengths in rings a and b are within the range of bond lengths seen in typical electron-delocalized systems, which are comparable to those in reported osmapentalenes (47). The substituted Cl in ring a is bonded to the central Os atom to form an unsaturated three-membered metallacycle, with Cl1–Os1 bond lengths of 2.7343(11) Å, which are longer than the Cl2–Os1 bond lengths of 2.3700(11) Å. The Cl1–C7–Os1 angle is 96.8(2)°, which is close to the X–C–Os angles reported in unsaturated metallaiodirenium ions and metallabromirenium ions [94.2(3)° and 95.8(5)°, respectively (48)].

NMR spectroscopic studies showed that complex **2** was stable in the reaction mixture overnight at ambient temperature under a nitrogen atmosphere, but after workup, including the addition of diethyl ether, the reaction mixture gave rise to new product **3** (Fig. 2). The ^{1}H NMR spectrum of an isolated sample of **3** displayed only two downfield chemical shifts at 9.44 and 7.70 ppm, indicating the considerable change in ring b compared to complex **2**. As reflected by the ^{13}C{^{1}H} NMR spectrum, one of the carbons in the metallacycles exhibited an obvious downfield shift to 325.3 ppm, close to the values previously reported for osmapentalyne (27). The formulation of **3** was further confirmed by single-crystal X-ray diffraction (Fig. 1*B*). The C1–Os1 bond length [1.865(9) Å] is much shorter than the C1–Os1 bond length in **2** [2.002(5) Å] but is comparable to the Os≡C bond length in osmapentalenes, indicating some triple bond character. Clearly supported by the Cl1–C7–Os1 angle [120.3(5)°], which is noticeably larger than that in **2** [96.8(2)°], the original, unsaturated, and three-membered metallacycle in **2** underwent a ring-opening process. We infer that diethyl ether acts as a Lewis base to deprotonate osmapentalene (**2**), resulting in the formation of the osmapentalyne (**3**). Interestingly, the addition of HBF_4 to a dichloromethane (DCM) solution of **3** led to the quantitative regeneration of **2**.

Natural bond orbital analysis of **2** at the B3LYP/6–31G* level with Stuttgart-Dresden-Bonn relativistic effective core potentials (SDD) for the Os atom revealed that the Wiberg bond indices (49, 50) for the bonds within the three-membered ring are 0.361 (Os1–Cl1), 1.030 (Os1–C7), and 1.095 (Cl1–C7). These values are in agreement with the expected trend in resonance forms 2A and 2C, shown in Fig. 3*A*, suggesting dative Cl → Os bond character. The Cl1 atom (0.23 e) is positively charged, indicating that resonance forms 2B and 2D both of feature an unprecedented chlorirenium cation. The tensor components of the nucleus-independent chemical shift (NICS) (51, 52) tensors for total NICS(1), NICS(0), NICS$_\pi$, and MO-NICS were studied (*SI Appendix*, Table S4). The computed NICS values for the three-membered ring in **2'** and **4'** [NICS(0) = −19.1 ppm for **2'** and −22.9 ppm for **4'**] unambiguously support the aromatic nature of the three-membered rings (NICS: B3LYP/6–31G* level with SDD for the Os atom) (53). Indeed, canonical molecular orbital NICS calculations (54) showed that the contributions to the NICS(0)$_{zz}$ value for the osmacyclopropene ring of **2'** from the π-molecular orbitals are +10.7 ppm, whereas the contribution from all the σ-orbitals is much more negative (−26.3 ppm), indicating σ-aromaticity in the osmacyclopropene ring. A similar bonding situation was also computed for unsaturated metallabromirenium ions (48). These experimental and computational studies indicate that the most plausible, electronic structure of **2** is a hybrid of four resonance forms (Fig. 3). Thus, **2** can be regarded as a cholorirenium cation consisting of a three-membered unsaturated ring skeleton.

As an alternative, bromobenzoiodaoxole was employed in an analogous fashion and participated in the bromination reaction of osmapentalene (**1**) (Fig. 2). Leaving a solution of **1** and 1-bromo-3,3-dimethyl-1,3-dihydro-1λ^3-benzo[*d*][1,2]iodaox-ole in DCM at RT for 10 min afforded an orange monobrominated compound (**4**). At RT, complex **4** was persistent for at least 1 wk in solution and was isolated in ∼81% yield. Compound **4** was also shown to undergo deprotonation with a Lewis base. The deprotonation was complete within 2 h to afford a osmapentalyne species (**5**) as a red solid in 79% yield. Both structures **4** and **5**

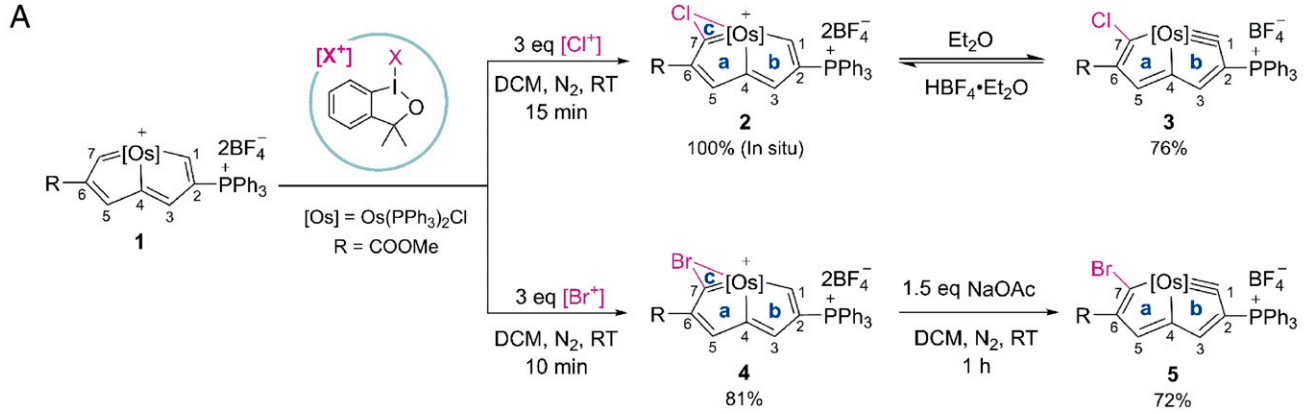

B

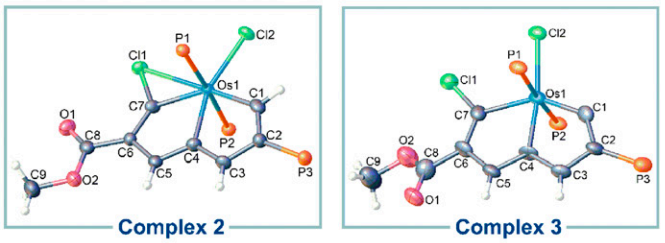

C

Complex **2**	C1	C2	C3	C4	C5	C6	C7
$^{13}C\{^1H\}$ NMR	226.4	138.7	162.8	188.7	165.2	150.1	224.6
Complex **3**	C1	C2	C3	C4	C5	C6	C7
$^{13}C\{^1H\}$ NMR	325.3	126.6	157.3	180.8	155.4	156.4	227.3

Note: unit (ppm)

D

Bond length	Os1-C1	C1-C2	C2-C3	C3-C4	C4-Os1	C4-C5	C5-C6	C6-C7	C7-Os1	C7-Cl1	Cl1-Os1	Os1-Cl2
Complex **2**	2.002(5)	1.372(7)	1.408(7)	1.377(7)	2.149(5)	1.386(7)	1.389(6)	1.387(6)	1.943(5)	1.708(4)	2.734(1)	2.370(1)
Complex **3**	1.865(9)	1.373(13)	1.394(12)	1.402(13)	2.087(8)	1.386(12)	1.410(13)	1.393(12)	2.113(8)	1.703(9)	3.318	2.445(2)

Bond angle	Os1-C1-C2	C1-C2-C3	C2-C3-C4	C3-C4-Os1	C4-Os1-C1	Os1-C4-C5	C4-C5-C6	C5-C6-C7	C6-C7-Os1
Complex **2**	124.4(4)	112.0(4)	113.0(4)	118.1(3)	72.59(19)	119.4(3)	113.3(4)	106.1(4)	132.1(3)
Complex **3**	130.2(7)	107.7(8)	112.4(7)	117.3(6)	72.5(4)	118.9(6)	114.9(8)	113.0(8)	118.7(6)

Bond angle	C7-Os1-C4	C7-Cl1-Os1	Cl1-Os1-C7	Os1-C7-Cl1
Complex **2**	68.98(19)	44.86(15)	38.33(13)	96.8(2)
Complex **3**	74.4(3)	33.346	26.351	120.4(5)

Note: bond length unit (Å), bond angle unit (°)

Fig. 2. (*A*) EAS reactions of osmapentalene. (*B*) The single-crystal structure of the cations of **2** and **3** at a 50% probability level. The phenyl groups in PPh_3 have been omitted for clarity. (*C*) Selected $^{13}C\{^1H\}$ NMR data for **2** and **3**. (*D*) Selected bond lengths and bond angles for **2** and **3**.

were confirmed unambiguously by X-ray crystallography (*SI Appendix*, Figs. S86 and S87). The structural parameters of **4** are very similar to those of reported metallabromirenium ions (48).

Collectively, these results demonstrate the EAS reactions of compounds with Craig-Möbius aromaticity via the halogenation reactions of osmapentalene. The deprotonation of the halogenation product **2** to give **3** and **4** to give **5** (Fig. 2) further demonstrates that the high strain allows for facile ring-opening reactions with Lewis bases of the three-membered ring.

EAS Reactions of Osmafuran-Fused Osmapentalene. While osmapentalene can undergo classical EAS reactions with halogen electrophiles, we speculated that fused osmapentalenes are suitable molecules for further investigation of the regioselectivity of EAS in Craig-Möbius aromatics. To obtain a general understanding of the regioselectivity, we first examined an analogous system with an aromatic ring fused in the Os-C7 position to exclude the high reactivity on C7. Treatment of complex 6, an osmafuran-fused osmapentalene (55), with 2 equivalents of 1-chloro-3,3-dimethyl-1,3-dihydro-1λ^3-benzo[*d*][1,2]-ioda-oxole or 1-bromo-3,3-dimethyl-1,3-dihydro-1λ^3-benzo[*d*][1,2]-iodaoxole at RT cleanly afforded complex **7** or complex **8** (Fig. 4*A*). After workup, **7** and **8** were isolated as blue-green powders in good yields. Both **7** and **8** produced only two diagnostic ^1H NMR resonances of metallaaromatics, indicating that they are disubstituted reaction products. The ^{13}C signals of C3 and C8 in **7** (127.7 and 111.9 ppm) and **8** (117.1 and 98.6 ppm) are at considerably higher fields than those of complex **6** (144.3 and 120.8 ppm), suggesting that disubstitution might have occurred at these two sites. The structure of **7** was further confirmed by a single-crystal X-ray diffraction investigation (Fig. 4*B*). These structural analyses clearly revealed that compound **7** contains a planar fused tricyclic structure, with two halogen atoms each substituted on the osmapentalene ring and osmafuran ring. The lengths of the

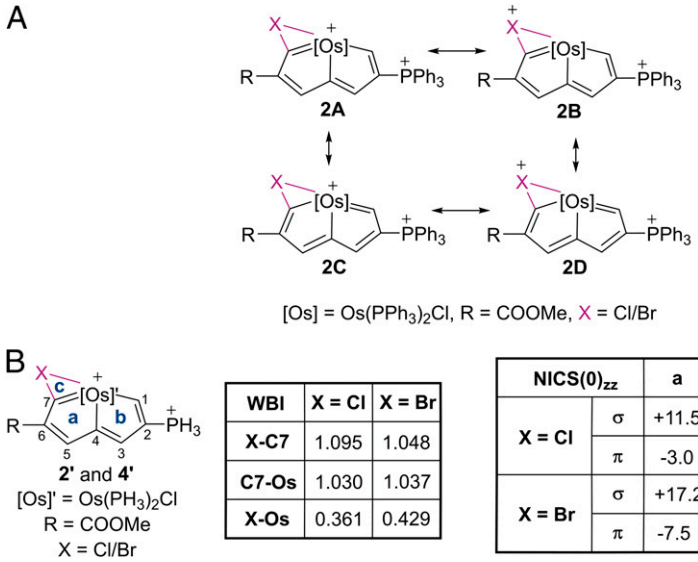

WBI	X = Cl	X = Br
X-C7	1.095	1.048
C7-Os	1.030	1.037
X-Os	0.361	0.429

$NICS(0)_{zz}$		a	b	c
X = Cl	σ	+11.5	+8.3	-26.3
	π	-3.0	-5.7	+10.7
X = Br	σ	+17.2	+15.6	-25.1
	π	-7.5	-12.8	+8.7

Fig. 3. (*A*) Four resonance forms for the cationic moieties of complex **2**. (*B*) Wiberg bond indices and NICS value of complexes **2′** and **4′**.

newly formed Cl–C bonds were found to be 1.746(10) and 1.749(11) Å.

When a solution of **6** and 1 equivalent of 1-chloro-3,3-dimethyl-1,3-dihydro-1λ^3-benzo[*d*] [1,2]-iodaoxole or 1-bromo-3,3-dimethyl-1,3-dihydro-1λ^3-benzo[*d*] [1,2]-iodaoxole in dichloromethane was stirred at RT for 6 h, complexes **9** and **10** formed and could be isolated as green solids in good yield (Fig. 4*A*). Experimentally, **9** and **10** could be converted to the final disubstitution products **7** and **8**, providing strong evidence for **9** and **10** as the key intermediates in the disubstitution reaction. X-ray diffraction studies revealed the formulation of **9** as monosubstitution product (Fig. 4*B*). The single chlorine substituent is located in the osmafuran ring with a Cl–C bond length of 1.762(8) Å.

To gain a better understanding of the high regioselectivity of the EAS reactions of osmafuran-fused osmapentalenes, the condensed Fukui function (56) derived from DFT was executed (Fig. 4*C*) to predict the most nucleophilic sites (atoms with the largest f_k^- value) in **6** and **7**. This method was successfully employed by Wright et al. to explain the observed nucleophilic substitution patterns and electrophilic substitution patterns for metallabenzenes and their derivatives (16, 19). The condensed Fukui functions for the cations of **6** and **9** were computed at the B3LYP/6–311G(d,p [d orbital and p orbital of heavy atom]) level of theory based on the model compounds **6** and **9**. As shown in Fig. 4*C*, the largest numerical value of f_k^- was found at C8 in the osmafuran ring of **6**, indicating that electrophilic attack at this atom is the most electronically favored. In the case of monosubstituted product **9**, the f_k^- value for C3 is much larger than that for the other two vacant sites, C1 and C5, which is in good agreement with the observed clear preference for attack at C3 in this compound. We infer that the steric effect might also play a role in the high regioselectivity of the EAS reactions of osmafuran-fused osmapentalene, although the electronic effect could be the most important factor.

The free-energy profiles of the C3 and C8 substitution reactions of **6** with chlorobenzo-iodaoxole are depicted in Fig. 4*D*. The C3 substitution reaction, affording **9b**, proceeds through transition state (TS) $\mathbf{TS_{6–9b}}$, with a free energy of 23.6 kcal/mol. C8 substitution product **9**, produced via $\mathbf{TS_{6–9}}$, has a lower energy barrier of 20.3 kcal/mol and thus forms readily. Although **9b** is the thermodynamic product, **9** cannot be converted to **9b** because the barrier for the conversion is inaccessible (48.4 kcal · mol^{-1}, which corresponds to the energy difference between **9** and $\mathbf{TS_{6–9b}}$). The monosubstituted compound **9** can revert to the final disubstituted product through $\mathbf{TS_{9–7}}$, with a computed barrier of 22.4 kcal/mol. Thus, kinetic control governs the substitution reactions of **6**, and only the initially formed C8 substitution product **9** is obtained.

We also carried out isotopic labeling experiments of **6** with deuterated trifluoracetic acid. As shown in Fig. 4*A*, the experiment suggested that electrophilic attack by an acid occurs preferentially at site C8 on osmafuran ring. The smaller deuterium substitution than halogen substitution at C8 further indicates that the electrophilic effect is predominant in the EAS of tricyclic compounds with Craig-Möbius aromaticity.

EAS Reactions of Osmabenzene-Fused Osmapentalene. Osmabenzene-fused osmapentalene with phenyl substituents was employed to further study the reactivity difference between osmabenzene and osmapentalene. As shown in Fig. 5*A*, treatment of complex **12** with 10 equivalents of Br_2 in dichloromethane solution (1.0 mol/L) led to the formation of **13**, which was isolated as a yellow-green solid in 55% yield. A single-crystal X-ray structure analysis revealed **13** to be the tetrasubstituted product of **12**, with two bromine atoms in the osmabenzene ring, one bromine atom in the osmapentalene ring, and one in the phenyl ring. Again, C3 was the only reactive site found in the osmapentalene ring, even when the reaction was performed with adequate electrophiles.

To clarify the reaction sequence, we carried out the halogenation reactions in steps. Upon gradual addition of one equivalent of a bromo reagent, such as a bromobenzoiodaoxole, bromine, or pyridinium tribromide, **14**, **15**, or **16**, respectively, were isolated as yellow-green powders, in moderate to high yields: **14**, 55%; **15**, 73%; **16**, 70%; and **13**, 62% (Fig. 5*B*). Single crystals of **13**, **14**, **15**, and **16** were investigated by X-ray diffraction to determine their structures. Plots for the cations of **13**, **14**, **15**, and **16** are shown in Fig. 5*C*, clearly indicating that they are tetra-, mono-, di-, and trisubstituted products, respectively. In all of these compounds, the metallabenzene-fused metallapentalene fragments are essentially coplanar, as suggested by the mean deviation from the least-squares plane of 12 atoms (0.040 Å for **13**, 0.038 Å for **14**, 0.031 Å for **15**, and 0.030 Å for **16**). A comparison of bond lengths and angles (*SI Appendix*, Figs. S87–S90) showed that they are all in the range of the corresponding quantities in osmabenzenes and osmapentalenes (57).

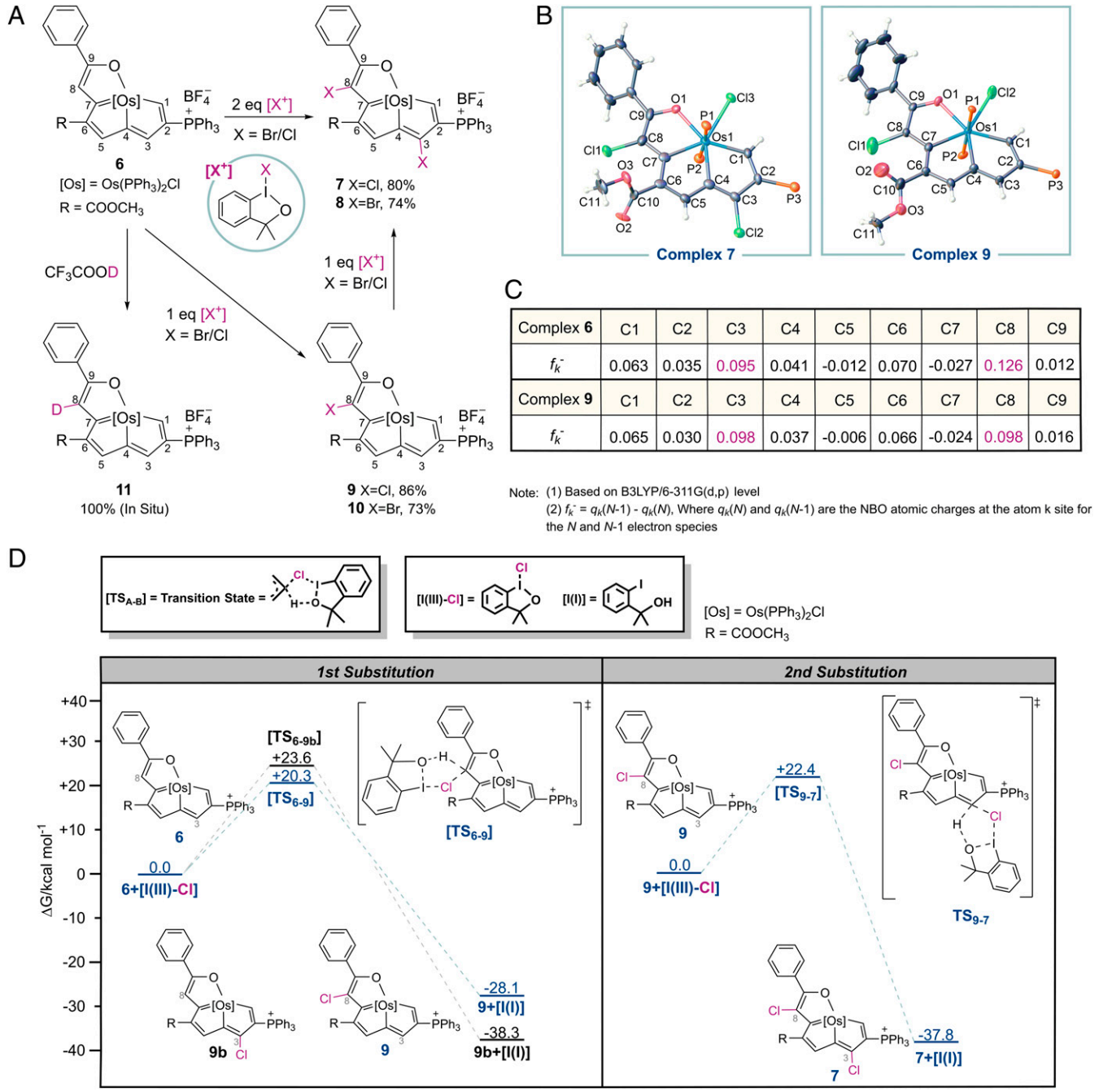

Fig. 4. (*A*) EAS reactions of osmafuran-fused osmapentalene with electrophilic reagents. (*B*) Single-crystal structure of the cations of **7** and **9** at a 50% probability level. The phenyl groups in PPh_3 are omitted for clarity. (*C*) Condensed Fukui function at different sites on complexes **6** and **9**. (*D*) Free-energy profiles of the C3 (black) and C8 (blue) substitution reactions. All energies are computed at the level M06L-D3/6–311G*/pcm//M06L-D3/6–31G*(SDD for Os, I), in kilocalorie/mole.

In contrast to the reaction of osmafuran-fused osmapentalene (**6**), the first halogenation reaction involves the osmapentalene ring of osmabenzene-fused osmapentalene (**12**). The differing positional selectivity for EAS reactions of **6** and **12** is attributed to the higher electron density of the osmafuran ring than that of in the osmapentalene and osmabenzene rings, respectively. The condensed Fukui function has also been employed to quantify the reactivity and positional selectivity for **12**. Consistent with the experimental findings, C3 has the largest f_k^- value in the case of **12**. The computed f_k^- values indicate that the second favorable site for electrophilic attack in metallacycles is C8, consistent with the structure of the isolated disubstituted product (**15**). However, the observed preference for the third substitution site (C13) can be traced to the phenyl group, which has a smaller f_k^- value than does the observed fourth substitution site in the osmabenzene ring (C10). In this case, C10 is sterically encumbered by adjacent bulky substituents, which preclude electrophilic attack by bromine-containing reagents. We speculate that the steric effect is an important factor affecting the competition for the third EAS site in **12**.

Additional DFT calculations were performed to study the formation of the substituted products. In the case of the first

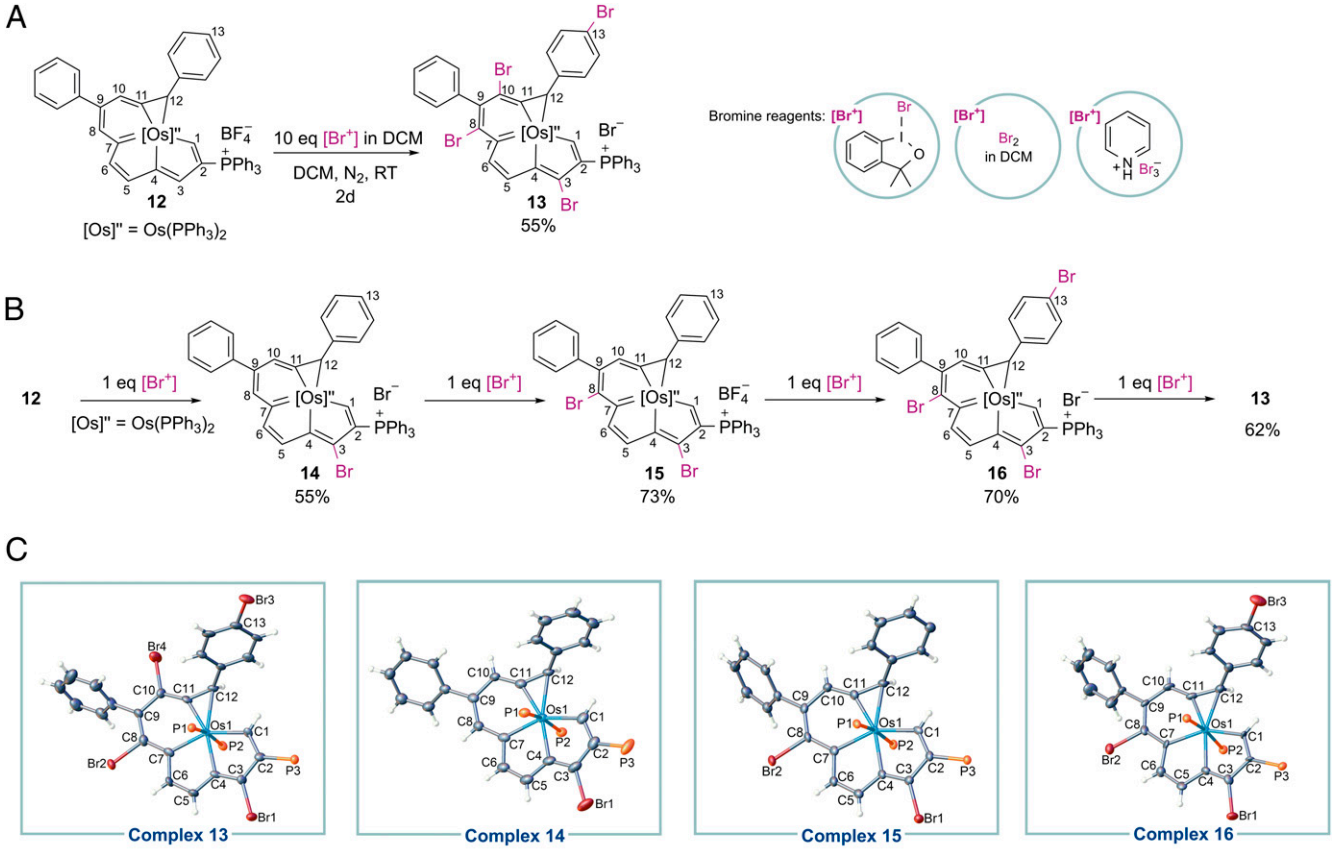

D

Complex **12**	C1	C2	C3	C4	C5	C6	C7	C8	C9	C10	C11	C12	C13
f_k^-	0.058	0.018	0.103	0.026	-0.002	0.042	-0.018	0.081	0.015	0.066	0.017	0.024	0.027
Complex **15**	C1	C2	C3	C4	C5	C6	C7	C8	C9	C10	C11	C12	C13
f_k^-	0.049	0.018	0.070	0.024	-0.001	0.039	-0.015	0.060	0.013	0.069	0.014	0.023	0.022

Note: (1) Based on B3LYP/6-311G(d,p) level
(2) $f_k^- = q_k(N\text{-}1) - q_k(N)$, Where $q_k(N)$ and $q_k(N\text{-}1)$ are the NBO atomic charges at the atom k site for the N and N-1 electron species

Fig. 5. (*A*) The electrophilic substitution reaction of osmabenzene-fused osmapentalene with a bromine cation. (*B*) Reactions of osmabenzene-fused osmapentalene with different equivalent electrophilic reagents. (*C*) The single-crystal structure of the cations of **13**, **14**, **15**, and **16** at a 50% probability level. The phenyl groups in PPh_3 are omitted for clarity. (*D*) Condensed Fukui function at different sites on complexes **12** and **15**.

substitution reaction of **12** (Fig. 6), the formation of **14** through $\mathbf{TS_{12–14}}$ is kinetically favorable with the free-energy barrier of 23.2 kcal/mol. In addition, **14** is more stable than the other three substitution products. Consistent with this theoretical result, only **14** was isolated and characterized experimentally. From **14**, disubstituted product **15** can readily form with a free energy of 16.3 kcal/mol through $\mathbf{TS_{14–15}}$, which aligns well with the observed experimental results. The two calculated TSs for the third substitution reactions are designated $\mathbf{TS_{15–16}}$ (C13) and $\mathbf{TS_{15–16b}}$ (C10). $\mathbf{TS_{15–16}}$ is higher in energy than $\mathbf{TS_{15–16b}}$ ($\Delta\Delta G^{\ddagger}$ = 10.9 kcal/mol). Additionally, C13-substituted product **16** is more thermodynamically favored than the C10-substituted product **16b**. Consequently, the fourth substitution at C10 could result in the formation of the experimentally observed, thermodynamically more stable tetrasubstituted product **13**. In all cases, the lowest-energy TSs lead to the experimentally observed mono-, di-, tri, and tetrasubstituted products.

Combined experimental and theoretical investigations have revealed the reactivity and positional selectivity in EAS reactions of osmapentalene and osmapentalene derivatives following classical EAS reactions. The positions with higher electron density are susceptible to electrophilic attack, although this increased reactivity might be offset by steric hindrance between substituents and electrophiles.

Conclusion

We have presented the possibilities and limitations of the application of EAS to osmapentalene species with Craig-Möbius aromaticity. Utilization of halogen reagents afforded several unprecedented metallacyclic species, such as unsaturated chloriridium ions. With fused osmapentalenes, however, electrophilic attack at the osmapentalene moiety affording halogen-substituted osmapentalene was observed, and an EAS reaction proceeded with fused osmafuran and fused osmabenzene rings, with the isolation of polysubstituted products. Control experiments led to the isolation of a series of stepwise-substituted products. Similar to the classical EAS reaction, both the electronic effect and the steric effect are linked to the EAS reactivity and regioselectivity, as evidenced by the results of DFT calculations. The EAS reactions of these Craig-Möbius aromatics

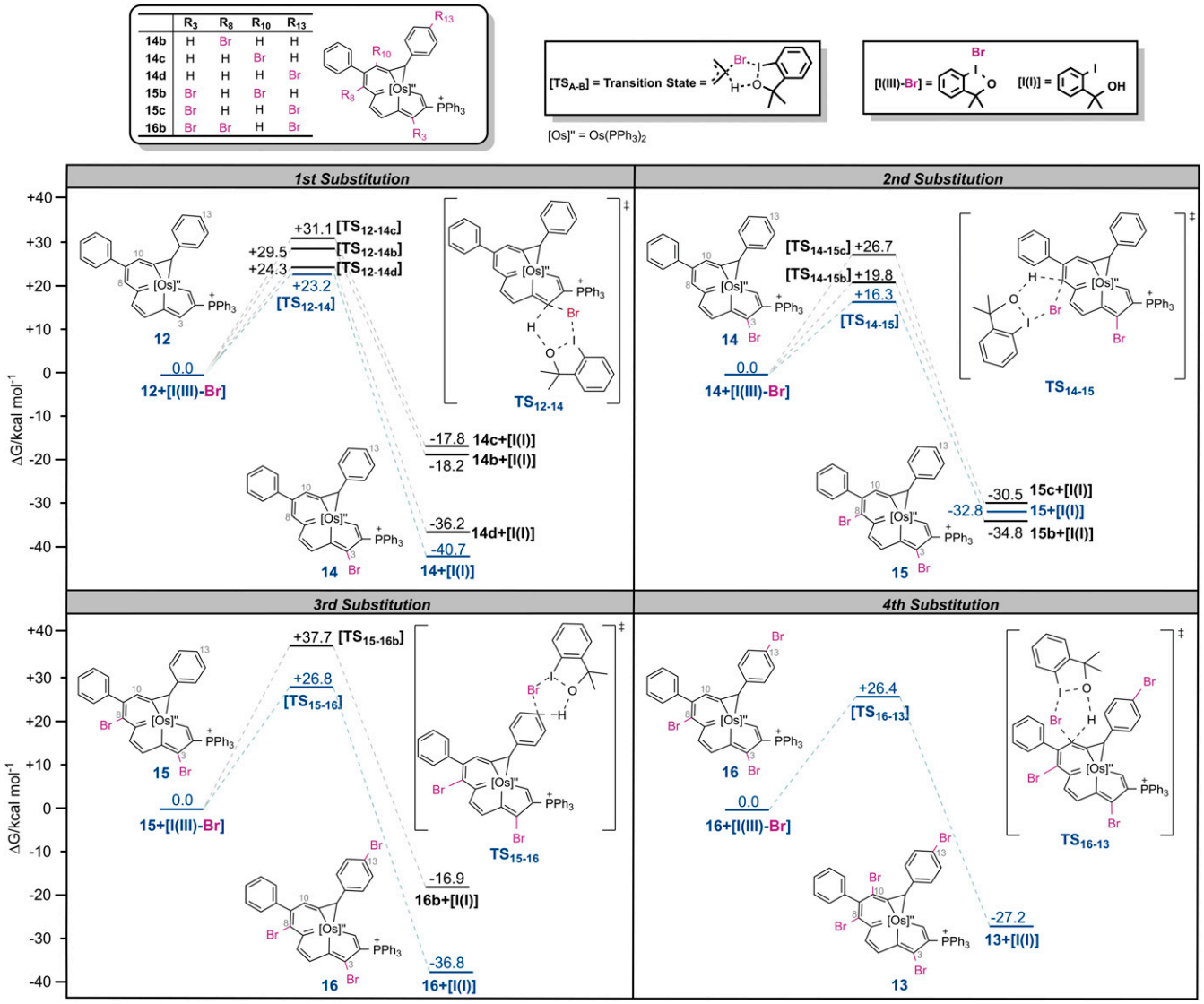

Fig. 6. Free-energy profiles of the possible substitution reactions of osmabenzene-fused osmapentalene **12**. All energies were computed at the level M06L-D3/6–311G*/pcm//M06L-D3/6–31G*(SSD for Os, I), in kilocalorie/mole.

represent an extension of the experimental indicator of aromaticity for Möbius aromatics. Perhaps more importantly, the understanding of where the reactivity of transition metal–containing aromatic compounds falls in the stability continuum from Hückel aromaticity to this less common Möbius aromaticity has been increased.

Materials and Methods

All syntheses were carried out under an inert atmosphere (nitrogen or argon) using standard Schlenk techniques unless otherwise stated. Solvents were distilled under nitrogen from sodium/benzophenone (hexane and diethyl ether) or calcium hydride (dichloromethane) prior to use. The 7C-carbolong compound **1** (47), 9C+1O carbolong compound **6** (55), and 12C-carbolong compound **12** (57) were synthesized according to the published literatures, and other reagents were used as received from commercial sources without further purification. All the calculations were performed with the Gaussian 09 software package. For computational details, refer to the *SI Appendix*.

Data Availability. All study data are included in the article and/or *SI Appendix*.

ACKNOWLEDGMENTS. We gratefully thank Prof. Kendall N. Houk (University of California Los Angeles) for his critical and insightful discussion. We also gratefully acknowledged Center for Computational Science and Engineering at Southern University of Science and Technology for the support of computational calculation resource. H.X. and H.Z. acknowledged the funding from the National Natural Science Foundation of China (Grant Nos. 21931002, 21871225, and U1705254) and the Fundamental Research Funds for the Central University (Grant No. 20720190042).

1. T. M. Krygowsi, M. K. Cyranski, Z. Häfilinger, G. Hafelinger, A. R. Katritzky, Aromaticity: A theoretical concept of immense practical importance. *Tetrahedron* **13**, 1783–1796 (2000).
2. S. F. Mason, New types of aromaticity. *Nature* **205**, 495–496 (1965).
3. E. Hückel, Quantum-theoretical contributions to the benzene problem. I. The electron configuration of benzene and related compounds. *Z. Phys.* **70**, 204–286 (1931).
4. E. Heilbronner, Hückel molecular orbittals of Möbius-type conformations of annulenes. *Tetrahedron Lett.* **5**, 1923–1928 (1964).
5. P. R. Schleyer, Introduction: Aromaticity. *Chem. Rev.* **101**, 1115–1118 (2001).
6. D. L. Thorn, R. Hoffmann, Delocalization in metallacycles. *Nouv. J. Chim.* **3**, 39–45 (1979).
7. J. R. Bleeke, Metallabenzenes. *Chem. Rev.* **101**, 1205–1227 (2001).
8. I. Fernández, G. Frenking, G. Merino, Aromaticity of metallabenzenes and related compounds. *Chem. Soc. Rev.* **44**, 6452–6463 (2015).
9. B. J. Frogley, L. J. Wright, Recet advances in metallaaromatic chemistry. *Chemistry* **24**, 2025–2038 (2018).

10. D. Chen, Y. Hua, H. Xia, Metallaaromatic chemistry: History and development. *Chem. Rev.* **120**, 12994–13086 (2020).
11. J. Chen, G. Jia, Recent development in the chemistry of transition metal-containing metallabenzenes and metallabenzynes. *Coord. Chem. Rev.* **257**, 2491–2521 (2013).
12. W.-X. Zhang, S. Zhang, Z. Xi, Zirconocene and Si-tethered diynes: A happy match directed toward organometallic chemistry and organic synthesis. *Acc. Chem. Res.* **44**, 541–551 (2011).
13. X.-Y. Cao, Q. Zhao, Z. Lin, H. Xia, The chemistry of aromatic osmacycles. *Acc. Chem. Res.* **47**, 341–354 (2014).
14. L. J. Wright, *Metallabenzenes: An Expert View* (John Wiley & Sons Ltd, 2017).
15. X. Zhou, H. Zhang, Reactions of metal-carbon bonds within six-membered metallaaromatic rings. *Chemistry* **24**, 8962–8973 (2018).
16. G. R. Clark, P. M. Johns, W. R. Roper, T. Söhnel, L. J. Wright, Regioselective mono-, di-, and trifunctionalization of Iridabenzofurans through electrophilic substitution reactions. *Organometallics* **30**, 129–138 (2011).
17. T. B. Wen *et al*., Protonation and bromination of an osmabenzyne: Reactions leading to the formation of new metallabenzynes. *J. Am. Chem. Soc.* **125**, 884–885 (2003).
18. W. Y. Hung *et al*., Electrophilic substitution reactions of metallabenzynes. *J. Am. Chem. Soc.* **133**, 18350–18360 (2011).
19. G. R. Clark, L. A. Ferguson, A. E. McIntosh, T. Söhnel, L. J. Wright, Functionalization of metallabenzenes through nucleophilic aromatic substitution of hydrogen. *J. Am. Chem. Soc.* **132**, 13443–13452 (2010).
20. R. Lin, H. Zhang, S. Li, J. Wang, H. Xia, New highly stable metallabenzenes via nucleophilic aromatic substitution reaction. *Chemistry* **17**, 4223–4231 (2011).
21. T. Wang *et al*., cine-Substitution reactions of metallabenzenes: An experimental and computational study. *Chemistry* **19**, 10982–10991 (2013).
22. W. Ma *et al*., Metallacyclopentadienes: Synthesis, structure and reactivity. *Chem. Soc. Rev.* **46**, 1160–1192 (2017).
23. M. Saito, Transition-metal complexes featuring dianionic heavy group 14 elements aromatic ligands. *Acc. Chem. Res.* **51**, 160–169 (2018).
24. M. Cui, R. Lin, G. Jia, Chemistry of metallacyclobutadienes. *Chem. Asian J.* **13**, 895–912 (2018).
25. J. Wei, W.-X. Zhang, Z. Xi, The aromatic dianion metalloles. *Chem. Sci. (Camb.)* **9**, 560–568 (2017).
26. D. P. Craig, N. L. Paddock, A novel type of aromaticity. *Nature* **181**, 1052–1053 (1958).
27. C. Zhu *et al*., Stabilization of anti-aromatic and strained five-membered rings with a transition metal. *Nat. Chem.* **5**, 698–703 (2013).
28. M. Mauksch, S. B. Tsogoeva, Demonstration of "Möbius" aromaticity in planar metallacycles. *Chemistry* **16**, 7843–7851 (2010).
29. K. An, T. Shen, J. Zhu, Craig-type Möbius aromaticity and antiaromaticity in dimetalla [10]annulenes: A metal-induced Yin-and-Yang pair. *Organometallics* **36**, 3199–3204 (2017).
30. J. Zhu, Open questions on aromaticity in organometallics. *Commun. Chem.* **3**, 161 (2020).
31. M. Mauksch, V. Gogonea, H. Jiao, P. V. R. Schleyer, Monocyclic $(CH)_9^+$ -A heilbronner Möbius aromatic system revealed. *Angew. Chem. Int. Ed. Engl.* **37**, 2395–2397 (1998).
32. H. S. Rzepa, Möbius aromaticity and delocalization. *Chem. Rev.* **105**, 3697–3715 (2005).
33. R. Herges, Topology in chemistry: Designing Möbius molecules. *Chem. Rev.* **106**, 4820–4842 (2006).
34. T. Tanaka, A. Osuka, Chemistry of meso-aryl-substituted expanded porphyrins: Aromaticity and molecular twist. *Chem. Rev.* **117**, 2584–2640 (2017).
35. D. Chen, Q. Xie, J. Zhu, Unconventional aromaticity in organometallics. *Acc. Chem. Res.* **52**, 1449–1460 (2019).
36. L. F. Cheung, G. S. Kocheril, J. Czekner, L.-S. Wang, Observation of Möbius aromatic planar metallaborocycles. *J. Am. Chem. Soc.* **142**, 3356–3360 (2020).
37. J. Wu, K. An, T. Sun, J. Fan, J. Zhu, To be bridgehead or not to be? This is a question of metallabicycles on the interplay between aromaticity and ring strain. *Organometallics* **36**, 4896–4900 (2017).
38. M. Mauksch, S. B. Tsogoeva, Hückel and Möbius aromaticity in charged sigma complexes. *Chemistry* **25**, 7457–7462 (2019).
39. D. Ajami, O. Oeckler, A. Simon, R. Herges, Synthesis of a Möbius aromatic hydrocarbon. *Nature* **426**, 819–821 (2003).
40. G. R. Schaller *et al*., Design and synthesis of the first triply twisted Möbius annulene. *Nat. Chem.* **6**, 608–613 (2014).
41. K. S. Anju, M. Das, B. Adinarayana, C. H. Suresh, A. Srinivasan, *meso*-Aryl [20]π homoporphyrin: The simplest expanded porphyrin with the smallest Möbius topology. *Angew. Chem. Int. Ed. Engl.* **56**, 15667–15671 (2017).
42. J. I. Wu, I. Fernández, Pv. Schleyer, Description of aromaticity in porphyrinoids. *J. Am. Chem. Soc.* **135**, 315–321 (2013).
43. A. Q. Cusumano, W. A. Goddard 3rd, B. M. Stoltz, The transition metal catalyzed [π2s + π2s + σ2s + σ2s] pericyclic reaction: Woodward-Hoffmann rules, aromaticity, and electron flow. *J. Am. Chem. Soc.* **142**, 19033–19039 (2020).
44. A. Yoshimura, V. V. Zhdankin, Advances in synthetic applications of hypervalent iodine compounds. *Chem. Rev.* **116**, 3328–3435 (2016).
45. V. V. Zhdankin, P. J. Stang, Chemistry of polyvalent iodine. *Chem. Rev.* **108**, 5299–5358 (2008).
46. R. Fu *et al*., DFT mechanistic study of methane mono-esterification by hypervalent iodine alkane oxidation process. *J. Phys. Chem. C* **123**, 15674–15684 (2019).
47. C. Zhu *et al*., Planar Möbius aromatic pentalenes incorporating 16 and 18 valence electron osmiums. *Nat. Commun.* **5**, 3265 (2014).
48. M. Luo, C. Zhu, L. Chen, H. Zhang, H. Xia, Halogenation of carbyne complexes: Isolation of unsaturated metallaiodirenium ion and metallabromirenium ion. *Chem. Sci. (Camb.)* **7**, 1815–1818 (2016).
49. I. Mayer, Bond order and valence indices: A personal account. *J. Comput. Chem.* **28**, 204–221 (2007).
50. D. Benitez *et al*., A bonding model for gold(I) carbene complexes. *Nat. Chem.* **1**, 482–486 (2009).
51. P. V. R. Schleyer, C. Maerker, A. Dransfeld, H. Jiao, N. J. R. van Eikema Hommes, Nucleus-independent chemical shifts: A simple and efficient aromaticity probe. *J. Am. Chem. Soc.* **118**, 6317–6318 (1996).
52. Z. Chen, C. S. Wannere, C. Corminboeuf, R. Puchta, Pv. Schleyer, Nucleus-independent chemical shifts (NICS) as an aromaticity criterion. *Chem. Rev.* **105**, 3842–3888 (2005).
53. S. Huzinaga *et al*., *Gaussian Basis Sets for Molecular Calculations* (Elsevier Science Publishing, Amsterdam, 1984).
54. C. Corminboeuf, T. Heine, G. Seifert, P. R. Schleyer, J. Weber, Induced magnetic fields in aromatic [*n*]-annulenes-interpretation of NICS tensor components. *Phys. Chem. Chem. Phys.* **6**, 273–376 (2004).
55. Z. Lu *et al*., Metallapentalenofurans and lactone-fused metallapentalynes. *Chemistry* **23**, 6426–6431 (2017).
56. N. Otero, M. Mandado, R. A. Mosquera, Revisiting the calculation of condensed Fukui functions using the quantum theory of atoms in molecules. *J. Chem. Phys.* **126**, 234108 (2007).
57. C. Zhu *et al*., CCCCC pentadentate chelates with planar Möbius aromaticity and unique properties. *Sci. Adv.* **2**, e1601031 (2016).